Freeze-Lining Formation in Submerged Arc Furnaces Producing Ferrochrome Alloy in South Africa

Joalet Dalene Steenkamp, Quinn Gareth Reynolds, Markus Wouter Erwee and Stefan Swanepoel

Abstract In 2016, a 63 MVA sub-merged arc furnace producing ferrochrome in South Africa was shut down and partially excavated for partial repair of its refractory lining as part of the annual maintenance activities. No significant evidence of the formation of a freeze-lining was found, although the lining design philosophy applied was of the conductive type typically applied. The paper presented here, investigate the possibility that the slag practice applied prior to excavation was not conducive to the formation and maintenance of a stable freeze-lining. The study included identification of the slag regimes under which the SAF was operated in the 12 months prior to the excavation, using data science techniques, and studying the effect of different regimes on freeze-lining behaviour, using transient one-dimensional heat transfer and thermodynamic models. Where available, temperature dependent properties for slag and refractory were utilised in the heat transfer calculations.

Keywords Excavation · Ferrochromium · Submerged arc · Furnace · Freeze-lining

Introduction

Ferrochrome alloy (FeCr) is essential to the production of stainless steel. In 2017, the global production of FeCr was 11.7 million tons with the main producers being China (39%), South Africa (29%), Kazakhstan (12%), and India (8%) [1]. A number

J. D. Steenkamp (✉) · Q. G. Reynolds · M. W. Erwee
MINTEK, Randburg, South Africa
e-mail: joalets@mintek.co.za

Q. G. Reynolds
e-mail: quinnr@mintek.co.za

M. W. Erwee
e-mail: markuse@mintek.co.za

S. Swanepoel
SamancorCr, Johannesburg, South Africa
e-mail: stefan.swanepoel@samancorcr.com

The Minerals, Metals & Materials Society (ed.), *TMS 2019 148th Annual Meeting & Exhibition Supplemental Proceedings*, The Minerals, Metals & Materials Series, https://doi.org/10.1007/978-3-030-05861-6_112

of grades of FeCr are available to producers of stainless steel, including high-carbon ferrochrome (HCFeCr) and charge chrome. HCFeCr typically contains 60–70% Cr and 4–6% C and charge chrome 50–55% Cr and 6–8% C. Charge chrome is produced in South Africa, due to the grades of the chromite ore available in the Eastern and Western Limb of the Bushveld complex [2, 3].

Either open arc furnace or submerged arc furnace (SAF) technology [4] is applied in the carbothermic reduction of chromite ores. To improve slag properties, slag conditioning is done through the addition of fluxes i.e. quartz, limestone, dolomite, or magnesite for improved slag/alloy separability and tap-ability of the slag amongst others [5, 6]. In South Africa, SAF technology is mainly applied where the electrode tips are submerged in a porous charge mix and the electrical energy primarily liberated by resistive heating [7] of the wet coke bed consisting of slag and carbonaceous reductant [8]. Thermally conductive lining design philosophies are typically applied [9]. In an open SAF, a gap exists between the top of the steel shell and the roof; the top of the burden is open to the atmosphere, and the CO-rich off-gas is combusted as it escapes. In a closed SAF, the roof is attached to the steel shell and the CO-rich off-gas is collected from an offtake on the roof for further treatment and use in downstream processes.

In the case study under investigation, an open 63 MVA SAF was shut down in 2016 for partial repair of its refractory lining as part of the annual maintenance activities. The lining design philosophy applied in this SAF was of the thermally conductive type [10]. The area of interest to the work presented here was the sidewall in the area where freeze-lining formation is expected. During partial excavation of the burden, to expose and remove the refractory that had to be replaced, no significant evidence of the formation of a freeze-lining was found. The absence of a freeze-lining could be attributed to a number of reasons including (a) the fact that the burden was melted down in preparation for the shutdown, (b) not all sections of the SAF was excavated nor was all of the parts excavated systematically studied so the freeze-lining could potentially have been present elsewhere, or (c) the slag practice applied prior to excavation was not conducive to the formation and maintenance of a stable freeze-lining.

The latter forms the basis of this paper in which the slag practice regimes under which the SAF was operated prior to the excavation was identified using machine learning techniques and the effect of the different regimes on freeze-lining behaviour was studied using heat transfer and thermodynamic models.

Identification of Significant Differences in Slag Practice Regimes

To investigate the significant differences in slag practice regimes, the per-tap slag analysis for a 12 month period prior to the furnace shutdown was examined, using data science techniques. The original dataset contained the slag analysis and calculated slag liquidus temperature (estimated using a proprietary calculation based on slag

composition) for 2416 taps. From the dataset captured per tap, seven main dimensions were selected for analysis: mass %Al_2O_3, %CaO, %MgO, %SiO_2, %FeO, and %Cr_2O_3 [5], as well as the slag liquidus temperature in degrees Celsius. Initial data validation indicated that there were 35 incidences where the total chemical analysis either exceeded 100% or was below 95%, and a further 16 incidences where no value was captured for %CaO. These instances were removed from the data set, leaving a total of 2365 tap analyses.

Typically, an investigation of this nature would rely on classical statistical methods to perform exploratory data analysis, using mean values to determine temperature dependent properties of slag if the underlying data was found to be normally distributed. However, it has to be noted that pyrometallurgical plants are notoriously complex in nature with operational performance being impacted by a multitude of variables [11]. Applying classical statistical methods and calculating the mean will therefore only partly describe the picture, and clusters of data that would meaningfully describe various slag regimes under which the furnace was operated, had to be identified.

Identification of the Clusters

Creating visual representations of multidimensional data is not simple and considerable time is often spent trying to determine whether there are well-defined groups in the data and whether or not any inter-relationships existed [12]. Also, there is a known tendency for analyst bias to impact the outcome of attempts to investigate and model the behavior of ferroalloy furnaces [13]. In order to identify well-defined groups and meaningful inter-relationships between them while limiting bias, data analysis was done using code developed in the open-source language, Python. Python libraries used were the pandas data analysis module [14], scikit-learn machine learning module [15], which was implemented by using a Jupyter notebook [16]. The seaborn: statistical data visualization library [17] was employed to assist with visualization. Due to promising results obtained in another study [18] the K-means algorithm was chosen to group the data into a pre-determined number of clusters in order to study the underlying structure of the data and identify salient features [19].

One of the discretionary parameters required for K-means clustering is the number of clusters to optimize for [20]. One method to assist in choosing the number of clusters is to run iterations of the algorithm, incrementally increasing the number of clusters and measuring the sum of squared distances between cluster centroids. The K-means sub-routine from the scikit-learn module captures this value as a parameter called ‘inertia’, and an incremental plot showing how this improves as the number of clusters increases is shown in Fig. 1a. The ‘elbow’ in the K-means inertia plot appears to be situated at three clusters, but a significant amount of improvement is still indicated when moving from three to four clusters. The improvement achieved by increasing clusters quickly decreases when going beyond four clusters. Principal component analysis (PCA) is a statistical technique for unsupervised

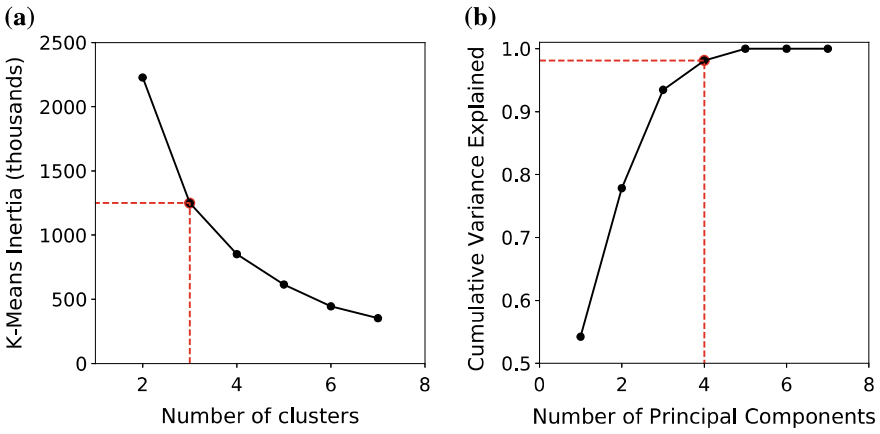

Fig. 1 Elbow plots for **a** the K-means algorithm to optimise the number of clusters and **b** the Principal Component Analysis technique applied to the plant data to assist with determining the number of principal components to search for in the data. Identifying the 'elbows' is subjective, and they appear to be situated at **a** three to four clusters or components

dimension reduction and has been argued to be related to K-means clustering [21]. In this instance, PCA was used to gain insight into the underlying structure of the data indicating that the original seven parameters could be compressed to four new components whilst still being able to explain 98% of the variance in the data—see Fig. 1b. As such, four clusters were chosen to perform the K-means clustering.

The result of the K-means clustering is that each tap analysis is allocated to one of the four clusters. The underlying 'meaning' of the clusters is not explicitly provided by the algorithm and may in fact not be present at all. The K-means algorithm will find clusters in any dataset, even when actual clusters in the data are not present and the clusters need to be validated. Further analysis and examination of the data is required to confirm that the groupings are sensible and that no large amount of overlap at the edges of the clusters occur (i.e. clusters should be discrete).

Validation of the Clusters

As a first step, the data was visualized to examine the densities of the individual clusters over the time period to determine if there were specific periods where a particular cluster dominated. It was found that slags from all clusters were present all the time.

Next the estimated slag liquidus temperatures for the 12 months was plotted as a function of time (represented by consecutive tap numbers), separating them into the clusters identified. The clusters appeared to be discrete with some overlap. As

different slag compositions would result in differences in liquidus temperatures, these results provided the first evidence of the validity of the clusters.

When the variables were plotted as scatterplots and the clusters stripped out, the structure of the discrete clusters became more apparent and demonstrated that segregation of the data occurred in more than one dimension. For example, Cluster 0 was typically higher in $\%Al_2O_3$ (Fig. 2a) and lower in $\%SiO_2$ (Fig. 2b) compared to the other clusters. In FeCr slags, variations in $\%Al_2O_3$ and $\%SiO_2$ contents would lead to variations in liquidus temperatures, as supported by the almost linear relationships where the liquidus temperature was proportional to the $\%Al_2O_3$ (Fig. 2c) and inversely proportional to the $\%SiO_2$ (Fig. 2d). These results provided further evidence of the validity of the clusters.

In addition to grouping each data point to a cluster, each cluster had a centroid location. The coordinates for the centroid location for each cluster represented the

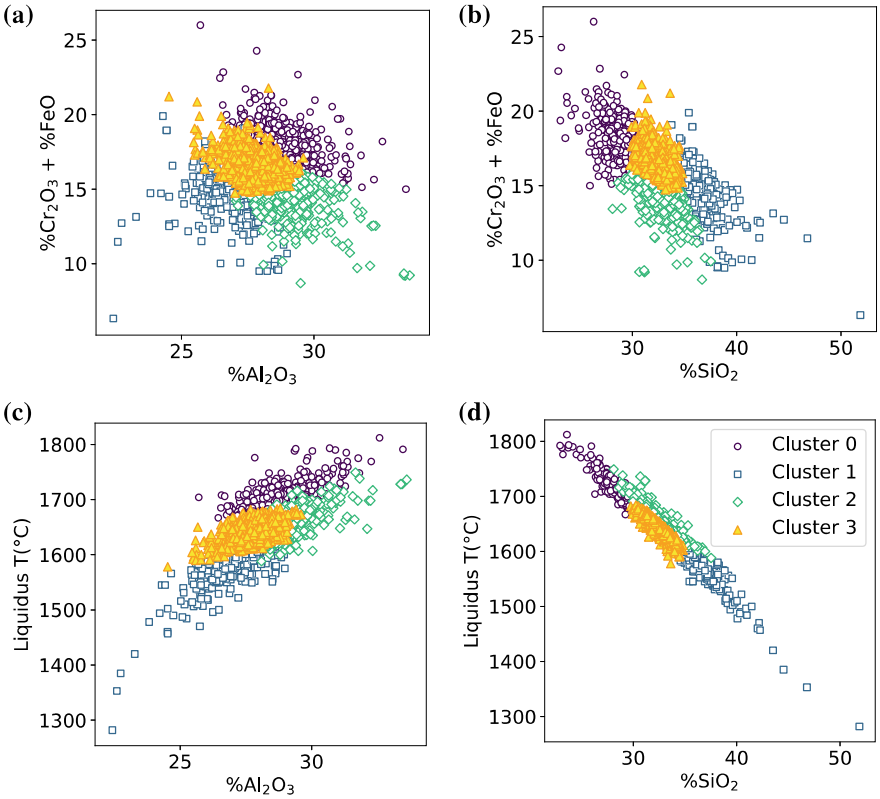

Fig. 2 Scatter plots for selected variables showing how the K-means identified clusters are grouped for multiple variable combinations. Firstly, for the combined mass$\%Cr_2O_3$ and %FeO against **a** the contained $\%Al_2O_3$ and **b** the contained $\%SiO_2$. And secondly, the estimated liquidus temperature **c** against contained $\%Al_2O_3$ and **d** contained $\%SiO_2$

chemical compositions applied in the following sections. A summary of the normalized four component analysis and relevant ratios were presented in Table 1. As illustrated in Fig. 3, the cluster centroids represented compositions that uniquely deviated from the mean analysis and provided further evidence of the validity of the clusters.

Table 1 Normalised four component analysis and relevant ratios of the four slag clusters that were identified by the K-means clustering algorithm and mean values of the total dataset. Due to confidentiality $\%Cr_2O_3$ and %FeO are not displayed separately

Cluster	$\%Al_2O_3$	%CaO	%MgO	$\%SiO_2$	$\frac{MgO}{Al_2O_3}$	$\frac{(MgO+CaO)}{Al_2O_3}$	$\frac{(Cr_2O_3+MgO+Al_2O_3)}{(FeO+SiO_2)}$
0	35.1	4.0	25.4	35.5	0.724	0.838	1.75
1	31.6	3.5	22.7	42.1	0.719	0.831	1.39
2	34.0	3.9	23.9	38.2	0.701	0.816	1.59
3	33.3	3.8	24.0	38.9	0.723	0.838	1.55
Dataset mean	33.5	3.8	24.0	38.7	0.718	0.832	1.56

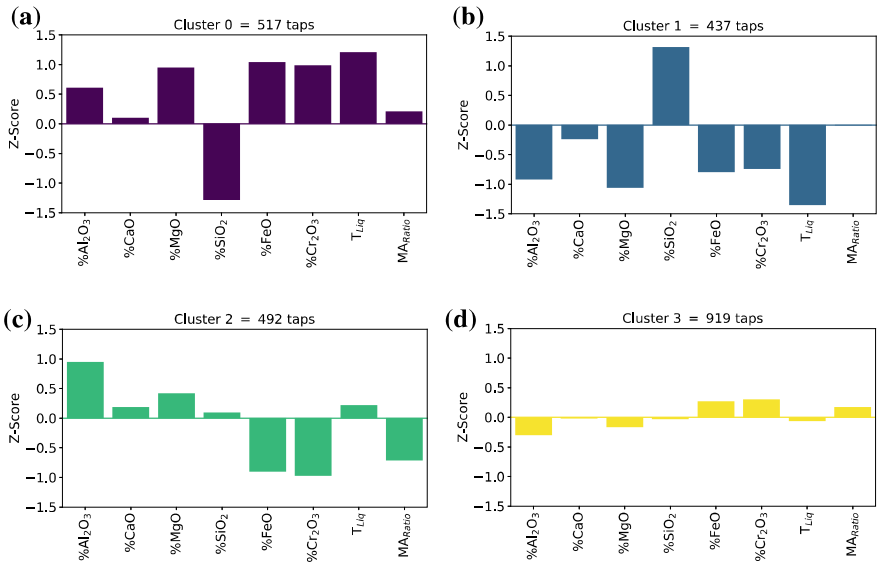

Fig. 3 Cluster sizes and centre coordinates (displayed as multiples of one standard deviation from the total mean values). MA Ratio is a ratio calculated by dividing %MgO by $\%Al_2O_3$. Z-scores were calculated by taking the difference between the cluster value and the dataset mean and then scaling this difference by the standard deviation of the dataset [22, 23]. The horizontal origin lines indicate where the mean of the total dataset is located, and the bars indicate the deviation from the dataset's mean expressed as multiples of the standard deviation of each variable

The final evidence of the four clusters was obtained by plotting 3-component projections by sequentially using a geometric transformation [24] on all the possible combinations of the slag components.

Development of Heat Transfer Model

In order to understand the effect of the different slag practice regimes on the thermal behaviour of the freeze-lining, a simple model of the furnace sidewall in the vicinity of the molten slag was developed. Although the patterns of energy transfer within a FeCr furnace are highly three-dimensional, the thickness of the sidewall is small in comparison to the rest of the dimensions of the furnace. Therefore, a locally one-dimensional (1D) approximation was deemed acceptable for a model intended for wide exploration of the system's behaviour. Furthermore, the validity of 1D-models in the study of freeze-linings was extensively explored by others and verified using experimental measurements (for example [25, 26]).

The sidewall refractory construction on which the 1D-model was based, was obtained from furnace drawings and dig-out reports: the general arrangement was shown schematically in Fig. 4. As refractory lining, the models were set up with 30 mm steel, 70 mm graphite refractory, 571 mm carbon refractory, and the thickness of the high alumina refractory was varied (0, 100, and 182 mm).

Development of Heat Transfer Model

In the absence of air gaps or other significant contact resistances, the primary mechanism of energy transfer would be conduction. Due to the large thermal mass and relatively poor thermal conductivity of the materials involved, transient effects can

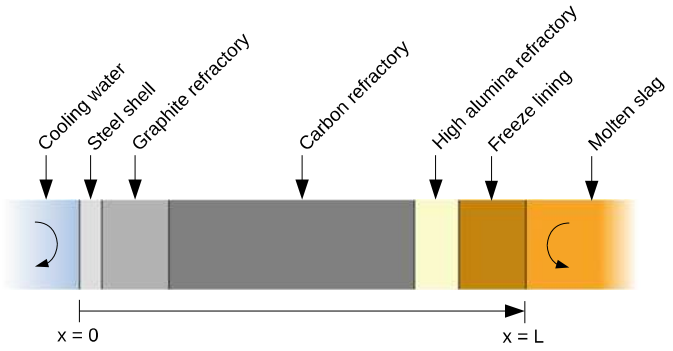

Fig. 4 Thermal freeze-lining model—section through furnace sidewall

be significant and were included here [27, 28]. The governing equation in such cases is a simple parabolic partial differential equation:

$$\rho C_P \frac{\partial T}{\partial t} = \frac{\partial}{\partial x} k \frac{\partial T}{\partial x} \tag{3}$$

Here T is the temperature field in K, described by position x and time t, ρ is the material density in kg/m^3, C_P is its specific heat capacity at constant pressure in J/kgK, and k is its thermal conductivity in W/mK. In general, the material properties are functions of both the type of material and the temperature, introducing some nonlinearity into (3) in the case of heterogeneous sidewall designs such as the one presented in Fig. 4.

In order to find a solution, the governing equation must also be provided with initial and boundary conditions. The initial temperature profile was set at either a constant value (cold sidewall start), or using values from a previous calculation (hot sidewall start). At the spatial boundaries, heat transfer coefficient relationships were imposed:

$$\text{At } x = 0: \quad k \frac{\partial T}{\partial x} = h_C (T - T_C) \tag{4}$$

$$\text{At } x = L: \begin{cases} k \frac{\partial T}{\partial x} = h_S (T_S - T) \\ T = T_{MPT} \end{cases} \tag{5}$$

Eq. (4) defines a heat transfer coefficient h_C between the sidewall cold face and the furnace cooling system, in this case a falling water film at bulk water temperature T_C. Equation (5) defines a heat transfer coefficient h_S between the sidewall hot face and the slag process temperature, given by T_S, unless the hot face was above the melting temperature of the freeze-lining or below the freezing temperature of the current molten slag, in which case a constant temperature boundary condition with the relevant value of T_{MPT} was applied. In the case where phase change was occurring, an additional equation then controlled the rate of change of the freeze-lining thickness, L:

$$\rho \lambda \frac{dL}{dt} = k \left. \frac{\partial T}{\partial x} \right|_L - h_S (T_S - T_{MPT}) \tag{6}$$

Here, λ is the enthalpy of fusion of the freeze-lining from the current molten slag (in the case of freezing) or the enthalpy of fusion of the freeze-lining (in the case of melting).

Equations (3)–(6) were integrated numerically using the finite volume method with backward-Euler time discretisation [28] in order to obtain a solution. The model was implemented in the Python programming language using high-performance sparse matrix solution methods from the Scipy scientific computing module [29]. The temperature solution at each time step was found on a moving mesh which was adjusted to the correct dimensions whenever the thickness of the freeze-lining

changed. Temperature-dependent material properties for the various refractory and freeze-lining components of the sidewall were stored on a high-resolution static mesh and linearly interpolated to locations on the moving mesh when required. An iterative predictor-corrector algorithm was used to reconcile Eq. (6) with the conductive heat transfer solution at every time step. Each individual model in the present work used fixed property meshes with 15,000 elements, moving meshes with 1,000 elements anisotropically biased toward the hot face, and up to 50,000 time-step solutions. Solution time on standard laptop PCs was of the order of a few minutes.

In order solve the 1D-model using Eqs. (3)–(6), the following variables had to be identified:

1. The temperature dependent properties:
   a. For the steel shell, three types of refractory materials (graphite, carbon, and high alumina) and the freeze-lining of various compositions: density (ρ), specific heat capacity at constant pressure (C_P), and thermal conductivity (k) as a function of temperature.
   b. The process temperature of slag (T_S) which will vary for different slag compositions.
   c. The melting temperature of the freeze-lining or freezing temperature of the current molten slag (T_{MPT}).
   d. The enthalpy of fusion (λ) of the solid freeze-lining material (in the case of melting) or of the solid phase precipitating from the current molten slag (in the case of freezing).
2. The heat transfer coefficients between the sidewall hot face and the process temperature of slag for various compositions (h_S) and between the sidewall cold face and the furnace cooling system (h_C).

Identification of Temperature Dependent Properties

Where applicable, temperature dependent properties were calculated using the Equilib module of FactSage™ 7.2 [30]. As databases, FactPS was selected for the gas and pure liquid and solid phases, and FTOxid for the solution phases. All the solution phases were considered in calculations. Where applicable, preference for data from the FTOxid database was given and duplicates suppressed. Temperature dependent properties that could not be calculated in FactSage™ were sourced from literature.

Density, Specific Heat Capacity, and Thermal Conductivity of Steel Shell and Refractory Materials

The density, specific heat capacity, and thermal conductivity of steel shell and refractory materials were summarized in Table 2. The data was mainly sourced from a

Table 2 Density, specific heat capacity, and thermal conductivity of steel shell and refractory materials

Property	Steel shell	Graphite refractory	Carbon refractory	High alumina refractory
ρ (kg/m^3)	7850	1630	1610	3000
C_P (J/kgK)	500	869 + 0.837 T	869 + 0.837 T	1129 + 0.108 T
k (W/mK)	45	140	18	1.5

number of textbooks [31–33] and validated against the specific data sheets from refractory suppliers. Note that for the purpose of solving the 1D-model, all of these properties were assumed to remain constant with changes in temperature. The one exception was the heat capacity for the refractory material (C_P) which was calculated in FactSage™ based on the assumption that the alumina refractory consisted of 59.7% Al_2O_3 and 40.3% SiO_2 (a typical composition for a high alumina refractory material).

Process Temperature

During operation, the six slag components (%Al_2O_3, %CaO, %MgO, %SiO_2, %FeO, and %Cr_2O_3) would be present as a liquid slag (containing MgO, Al_2O_3, SiO_2, and CaO) as well as partially altered chromite [6, 34, 35]. In South Africa, the partially altered chromite nominally consists of (Fe, Mg)Cr_2O_4 and represents the FeO and Cr_2O_3 present in the bulk slag analyses [6]. It is important to understand that partially altered chromite is almost always present in the slag, since full reduction of FeO_x and Cr_2O_3 and dissolution into the slag phase is limited.

As the actual process temperature was not known, a conservative estimate of the process temperature (T_S) was made by calculating the liquidus temperature of the slag in FactSage™, as if it included all six components under a reducing atmosphere. An oxygen partial pressure of 10^{-9} atm was assumed, based on typical oxygen pressures for chromite smelting [36].

Composition, Melting Point, Specific Heat Capacity, and Enthalpy of Fusion of Freeze-Lining

The potential composition of the freeze-lining for each slag cluster was derived from the solidification behaviour of each of the clusters as calculated in FactSage™ from 1900 °C (2173 K) to the solidus of the particular slag. The calculations were based on the assumption (and simplification) that the primary phase to precipitate from the liquid slag will form the freeze-lining. In this instance, only the 4-component slag was considered since these components make up roughly 90% of the slag and would be fully molten at the process temperature (T_S), whereas not all of the chromite

would have dissolved to form part of the freeze-lining. The results were presented in Fig. 5. In all instances, the primary phase to precipitate was spinel, more specifically $MgAl_2O_4$.

The melting point calculated for the four-component slag was used as the melting point of the freeze-lining (T_{MPT}) for each cluster involved. The enthalpy of fusion (ΔH) was also calculated during the solidification simulation and was the negative of the enthalpy of the liquid to solid reaction when spinel precipitated from the melt. The heat capacity of the spinel phase (C_P) was also extracted from the results of the solidification calculation and fitted as linear correlations of temperature for the four-component slag. The results were presented in Table 3.

Thermal Conductivity and Density of the Freeze-Lining

Estimation of the thermal conductivity (k) and density (ρ) of a freeze-lining is quite complex since porosity, grain size, and composition all influence these values to varying degrees. Furthermore, any other phase that would co-precipitate with the primary phase will change the phase composition of the lining and hence the thermal conductivity thereof. Although the thermal conductivity and density of oxides at

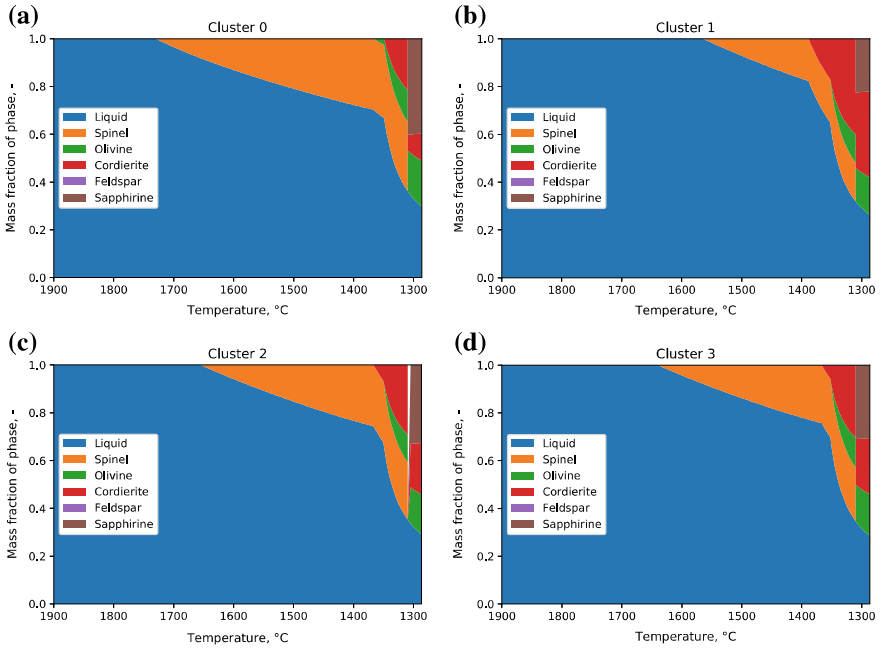

Fig. 5 Solidification behaviour of the four-component slag in the temperature range 1900–1300 °C (2173–1573 K). Ideal composition in this context: spinel = $MgAl_2O_4$, olivine = Mg_2SiO_4, cordierite = $Al_4Mg_2Si_5O_{18}$, feldspar = $CaAl_2Si_2O_5$, sapphirine = $Mg_4Al_{10}Si_2O_{23}$

Table 3 Calculated process temperature and melting point, specific heat capacity at constant pressure, and enthalpy associated with the solidification reaction representing the enthalpy of fusion of the freeze-lining for each cluster

Cluster	T_S (°C)	T_S (K)	T_{MPT} (°C)	T_{MPT} (K)	Cp (J/kgK)	ΔH or (λ) (kJ/kg) for liquid to solid reaction
0	1819	2092	1730	2003	0.601T + 413	−949
1	1736	2009	1565	1838	0.505T + 575	−517
2	1772	2045	1655	1928	0.558T + 486	−788
3	1780	2053	1641	1914	0.544T + 511	−755

high temperatures could be quite difficult to source, it was fortunately reasonably well documented for pure $MgAl_2O_4$ spinel. Therefore, thermal conductivity data for pure, non-porous $MgAl_2O_4$ was taken from the work by Wilkerson et al. [37], and for density from Kaprálik [38].

$$k = \frac{5492}{T} + 0.7492 \tag{1}$$

where k is the thermal conductivity in W/mK, and T, the temperature in Kelvin.

$$\rho_T = 3581.40 - \frac{1884.39}{10^5}T - \frac{5202.30}{10^9}T^2 \tag{2}$$

where ρ_T is the density in kg/m^3 and T, the temperature in Kelvin.

Identification of the Heat Transfer Coefficients

The heat transfer coefficient (h_S) was determined by grouping and analysing thermocouple data from plant measurements per slag cluster. The thermocouples in each differential pair were located in the carbon brick refractory, a known distance apart, which permitted the calculation of an energy flux through the sidewall assuming a steady state condition. This was then used, together with the process temperature differences, to estimate the heat transfer coefficient per cluster. The time-averaged readings from a set of differential thermocouples at positions in one of the high temperature areas were examined, with the highest average ΔT value being selected—this was assumed to indicate locations at which elevated thermal sidewall wear was likely. The results were shown in Table 4 and agree reasonably well with values proposed for similar applications by other authors [39].

Table 4 Calculation of process heat transfer coefficients in slag region

Condition	Thermocouple ΔT (K)	Slag $T_S - T_{MPT}$ (K)	Calculated h_S (W/m^2 K)
Cluster 0	68	89	106
Cluster 1	68	171	55
Cluster 2	72	117	85
Cluster 3	73	139	73

Values of h_c in film cooling arrangements are generally high, of the order of thousands of W/m^{2}K [39]. In the present work, an indicative value of 1,000 W/m^{2}K was used and resulted in temperature predictions which matched well with measurements taken from thermocouples in the furnace sidewall.

Quantification of Effect of Different Regimes on Freeze-Lining Behaviour

Freeze-Lining Formation from Different Slag Clusters

In order to explore the behaviour of each cluster individually the heat transfer models were run from a cold-start condition with no freeze-lining present, and with the refractories at room temperature (25 °C, 298 K). At the start of the simulation, the sidewall was exposed to the slag conditions associated with each cluster, and allowed to run until steady state was achieved. This exercise was conducted for several different thicknesses of the sacrificial alumina refractory in front of the carbon bricks, as part or all of this lining is expected to be consumed after initial start-up of the furnace [39]. The results were presented in Fig. 6 where the dashed black lines indicated the position of the refractory hot face, and the filled region above it the thickness of the freeze-lining.

For the case where no alumina refractory was present (Fig. 6a), freeze-lining formation would take a month or more, and the final steady state thicknesses ranged between 686 and 789 mm, with 103 mm being the largest difference between the clusters (cluster 3 vs. cluster 0). When an alumina refractory was present, the systems would reach steady state somewhat faster, and result in thinner freeze-linings:

- For the condition of a 100 mm thickness of alumina refractory on the sidewall (Fig. 6b), steady state would be reached after 15–20 days in most cases, and the final thickness ranged between 245 and 332 mm, with 87 mm being the largest difference between the clusters (again cluster 3 vs cluster 0). The maximum temperature observed in the alumina refractory across all clusters was 1047 °C (1320 K).

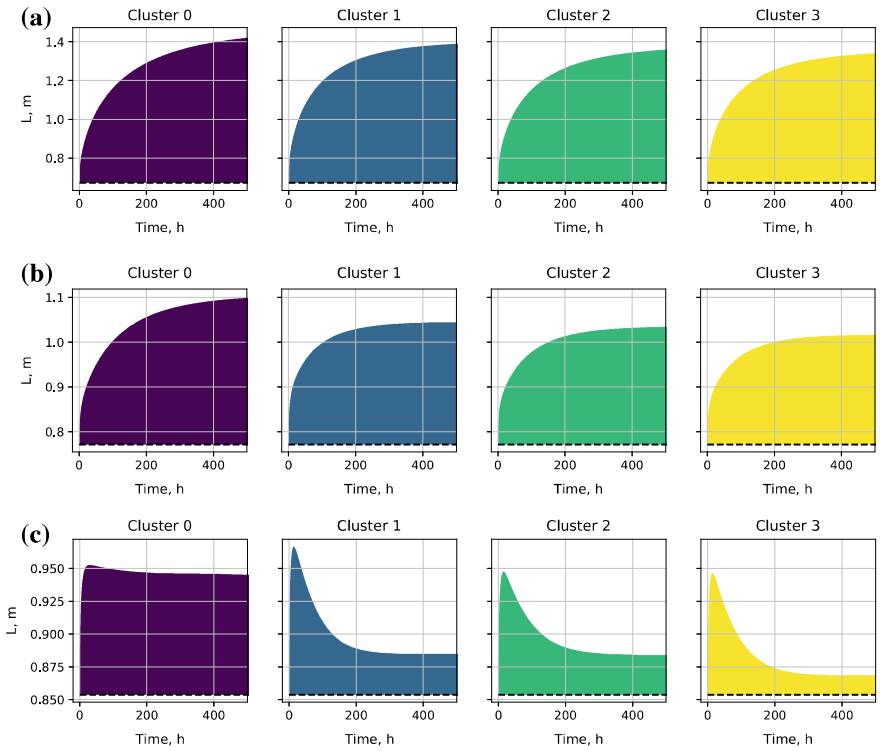

Fig. 6 Freeze-lining growth over time for each cluster model. **a** No alumina refractory is present and growth of the freeze-lining started at the hot face of the carbon refractory, 672 mm from the cold face of the steel shell. **b** 100 mm alumina refractory present and growth of the freeze-lining started at the hot face of the alumina refractory, 772 mm from the cold face of the steel shell. **c** 182 mm alumina refractory present and growth of the freeze-lining started at the hot face of the alumina refractory, 854 mm from the cold face of the steel shell

- For the condition of a 182 mm alumina refractory remaining on the sidewall (Fig. 6c), the sidewall would reach thermal equilibrium rapidly (typically less than 10 days) with substantial differences in the thickness between clusters, with cluster 0 showing the thickest lining at 93 mm and cluster 3 the thinnest at 15 mm.

The condition of a 182 mm alumina refractory corresponds to the condition at which the maximum temperature seen by the alumina refractory at steady state is at its liquidus temperature of 1600 °C (1873 K); this was therefore an estimate of the maximum stable quantity of alumina refractory that will remain on the sidewall during normal operation (based on the assumption that melting would be the wear mechanism applicable).

Interaction Effects

In the second phase of the heat transfer modelling exercise, interaction effects between different clusters were explored as significant movement between clusters were identified during the analyses of the tap data.

Two cases were investigated: (a) the potential for interaction under transient heat transfer conditions with the potential of melting only or (b) the potential for melting and dissolution at constant temperature (Fig. 7).

Interaction Effects Under Transient Heat Transfer Conditions

The analyses was performed by initialising a sidewall model with the steady-state values of temperature and freeze-lining thickness obtained previously, and placing it in contact with a molten slag from a different cluster. This resulted in a number of complex non-linear effects due to the differences in process and material parameters between clusters, as shown in Fig. 8 for the case of 182 mm alumina refractory. Similar interaction effects were seen in cases where less of the alumina refractory remains intact, however the time taken for the freeze linings to melt back and re-grow (in the cases where this happens) were longer.

When analysing Fig. 8, the freeze-lining behaviour when moving between any pair of clusters, could be grouped into three broad types:

1. The first type was characterised by extensive melting of the original freeze-lining followed by regrowth of a new freeze-lining. This occurred in the transitions from cluster 1 to 0, 1 to 2, 1 to 3, 2 to 0, 3 to 0, and 3 to 2. In most cases the melting phase was very rapid and lasted less than four hours. The regrowth phase was

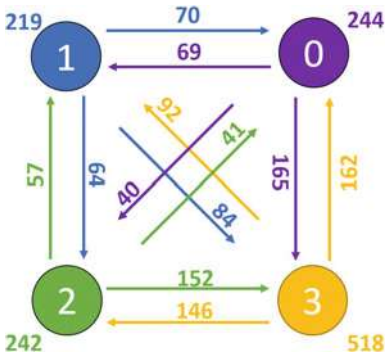

Fig. 7 Graphical representation of the movement between clusters per tap. Circles indicate the cluster number, whilst arrows indicate the direction of movement. The numbers next to the arrows indicates the number of taps that movement took place in the direction indicated. The numbers on the outside of the circles indicates the number of taps that no movement took place and taps remained steady in that cluster

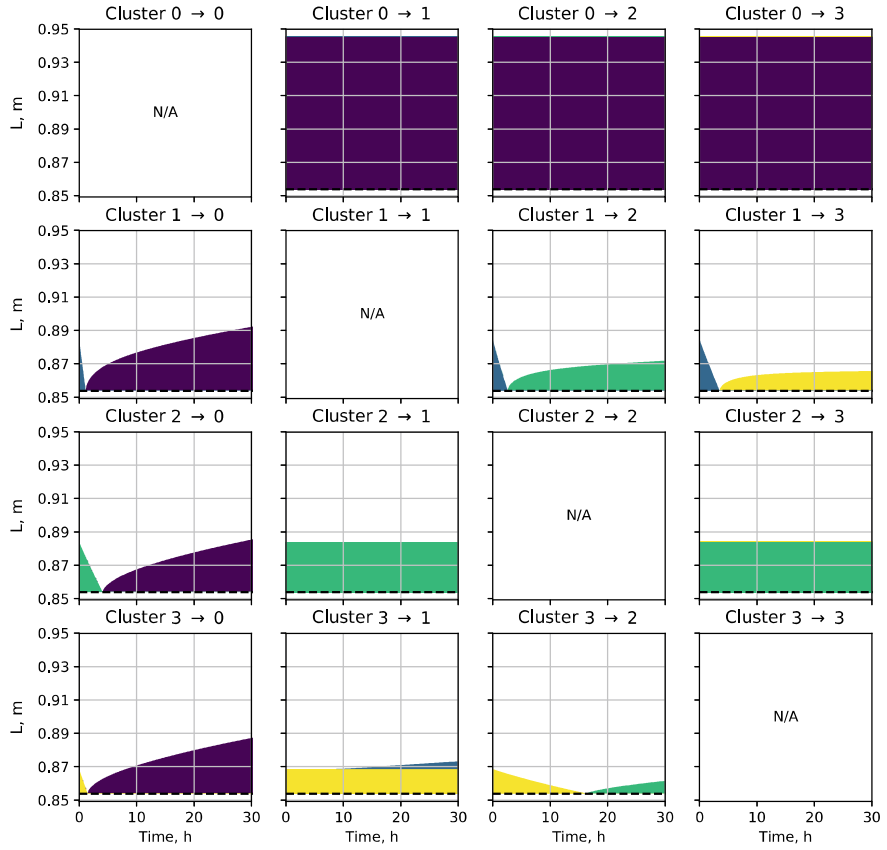

Fig. 8 Freeze-lining growth over time for interactions between different clusters, 182 mm alumina refractory present. Growth of the freeze-lining started at the hot face of the alumina refractory, 854 mm from the cold face of the steel shell

considerably slower, and could take up to a day or more to reach a new steady state.

2. The second type was characterized by the original freeze-lining material simply heating or cooling to some degree, leaving the second cluster's molten slag in direct contact with the frozen material from the first cluster. This occurred in transitions from cluster 0 to 1, 0 to 2, 0 to 3, 2 to 1, and 2 to 3. Because the molten slag was not at thermodynamic equilibrium with the solid freeze-lining material, chemical wear of the freeze-lining by slag was a possibility in these cases, as further discussed in the following section.
3. The third type of behaviour was characterised by material from the second cluster freezing a new layer over the material left by the first cluster, forming a heterogeneous lining. This occured only in the transition from cluster 3 to 1, and initial formation of the secondary freeze-lining took up to ten hours. Chemical wear of

the original freeze-lining was therefore also a possibility in the time immediately after this transition.

Potential for Chemical Wear at Constant Temperature

The potential for chemical wear by melting and dissolution of the freeze-lining, when liquid slag from any other cluster comes into contact with the freeze-lining phase, was calculated in FactSage™ 7.2 [30] using the same assumptions as described before. The results (Fig. 9) indicated how much of the existing freeze-lining (in all instances consisting of $MgAl_2O_4$ spinel only) would dissolve in 100 g of liquid slag from any other cluster at the process temperature of the slag (T_S) of a particular cluster. Higher amounts of liquid slag formation would hence imply that a higher amount of chemical wear was expected from that slag, until saturation in freeze-lining material occurs. It was evident from the results in Fig. 9, that the potential of dissolving some or all of the freeze-lining material was possible with all slags, but that some slags were much more aggressive. In order of worst to best, in terms of chemical wear: cluster 1, cluster 3, cluster 2, and then cluster 0. It is, however, extremely important to note that the potential for chemical wear cannot be isolated from heat transfer effects in the furnace.

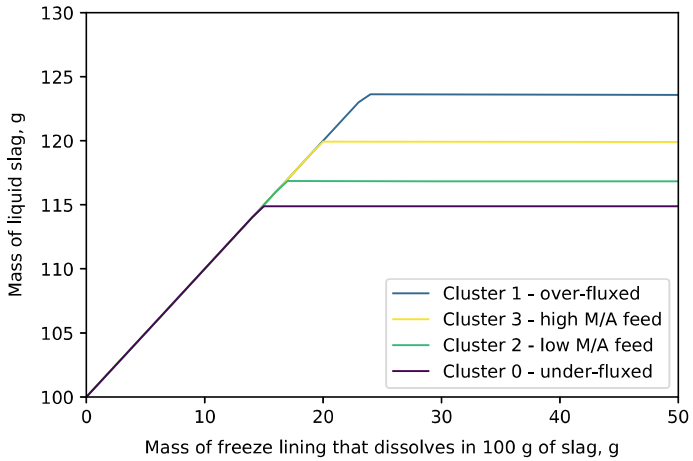

Fig. 9 Potential for chemical wear of freeze-lining (consisting of $MgAl_2O_4$ spinel only) interacting with slag from each cluster where under-fluxed slag did not contain sufficient SiO_2 to lower liquidus [4] to target range, over-fluxed slag contained too much SiO_2 resulting in a liquidus temperature below target range, low M/A feed was adequately fluxed (liquidus within target range) but the ore had lower MgO/Al_2O_3 ratio, and high M/A feed adequately fluxed (liquidus within target range) but the ore had higher MgO/Al_2O_3 ratio

Conclusion

During the partial excavation of an open SAF utilised in FeCr production no significant evidence of the formation of a freeze-lining was found. The study presented here investigated the potential for the slag practice applied prior to excavation to be the cause.

Using data science techniques, the compositions of tapped slag were clustered into four clusters. K-means clustering is a simple tool that can assist in analysing pyrometallurgical plant information, such as slag analyses. The ability to identify the clusters of slag greatly enhanced the analyses that could be performed on the data than would have been possible if only the mean values were considered.

Heat transfer calculations indicated that the sacrificial alumina refractory layer on the hot face of the refractory lining could play a significant role in the rate at which the initial freeze-lining formed, as well as the final thickness and therefore stability of the freeze-lining. The implications of these observations in terms of the refractory design, more specifically when specifying the type and thickness of the sacrificial lining, would be interesting to consider. It is important to note that the potential for the high alumina refractory to interact with the slag of various compositions were not investigated.

Heat transfer calculations further indicated that changing from one slag regime to another could negatively influence the stability of the existing freeze-lining. The only freeze-lining for which it was not the case was the under-fluxed slag. From a chemical wear perspective, the freeze-lining formed from under-fluxed slag was also most stable. In the case of furnace start-up particularly, the thermal behaviour of the sidewall refractory and freeze lining can be extremely complex, with material first freezing on to the cold refractories and then melting back as the system reaches thermal equilibrium, often at the expense of some or all of the sacrificial alumina refractory layer. More advanced thermal and chemical models building on the methods demonstrated in this paper may permit management of the start-up process to ensure a consistent build-up of freeze lining material, while minimising the thermal and chemical damage of the sidewall.

It is clear that both the dynamic and steady state behaviour of even very simple freeze-lining models is highly complex when transitions between multiple materials and operating conditions are considered. Such models are also very sensitive to many of the parameters used. Small errors in, for example, the sidewall design with regard to insulating components such as high alumina refractory, or refractory and freeze-lining properties such as thermal conductivity, may have a significant impact on the results. Further experimental and theoretical study of particularly the temperature dependent properties of the materials found in operating furnaces is highly recommended in order for freeze-lining models to provide reliable quantitative predictions in the future.

Lastly, systematic excavation of industrial SAFs, shutdown under full load and allowed to cool down, would provide invaluable information with regards to the actual formation and composition of freeze-linings in FeCr production.

Acknowledgements The paper is published with the permission of MINTEK and Samancor^{Cr}.

References

1. Pariser HH, Backeberg NR, Masson OCM, Bedder JCM (2018) Changing nickel and chromium stainless steel markets—a review. J South Afr Inst Min Metall 118(6):563–568
2. Cramer LA, Basson J, Nelson LR (2004) The impact of platinum production from UG2 ore on ferrochrome production in South Africa. J South Afr Inst Min Metall 104(9):517–527
3. Geldenhuys IJ (2013) Aspects of DC chromite smelting at MINTEK—an overview. Paper presented at INFACON XIII, Almaty, Kazakhstan 9–12 June 2013
4. Mc Dougall I (2013) Ferroalloys processing equipment. In: Gasik MI (ed) Handbook of ferroalloys: theory and technology. Butterworth-Heinemann, Oxford, pp 83–138
5. Jones RT, Erwee MW (2016) Simulation of ferro-alloy smelting in DC arc furnaces using Pyrosim and FactSage. CALPHAD: Comput Coupling Phase Diag Thermochem 55:20–25
6. Hayes PC (2004) Aspects of SAF smelting of ferrochrome. Paper presented at INFACON X, Cape Town, South Africa 1–4 February 2004
7. Barker IJ Rennie MS, Hockaday CJ, Brereton-Stiles PJ (2007) Measurement and control of arcing in a submerged-arc furnace. Paper presented at INFACON XI, New Delhi, India 18–21 February 2007
8. Ringdalen E, Eilertsen J (2001) Excavation of a 54 MVA HC-ferrochromium furnace. Paper presented at INFACON IX, Quebec City, Canada 3–6 June 2001
9. Coetzee C, Duncanson PL, Sylven P (2010) Campaign extensions for ferroalloy furnaces with improved tap hole repair system. Paper presented at INFACON XII, Helsinki, Finland 6–9 June 2010
10. Coetzee C, Sylven P (2010) No taphole—no furnace. Paper presented at refractories 2010 conference, Misty Hills, South Africa 16–17 March 2010
11. Yang Y, Xiao Y, Reuter MA (2004) Analysis of transport phenomena in submerged arc furnace for ferrochrome production. Paper presented at INFACON X, Cape Town, South Africa 1–4 February 2004
12. Poco J et al (2011) A framework for exploring multidimensional data with 3D projections. Paper presented at Eurographics/EuroVis 2011, Bergen, Norway 31 May 3 June 2011
13. Eksteen JJ, Frank SJ, Reuter MA (2004) Towards predictive control of ferroalloy furnaces: combining thermochemistry, inventory modelling and systems engineering. Paper presented at INFACON X, Cape Town, South Africa 1–4 February 2004
14. Python data analysis library (2018) https://pandas.pydata.org/. Accessed 6 Sept 2018
15. Pedregosa F et al (2011) Scikit-learn: machine learning in Python. J Mach Learn Res 12:2825–2830
16. Kluyver T et al (2016) Jupyter notebooks—a publishing format for reproducible computational workflows. Open Access 87–90
17. Waskom M et al (2014) Seaborn: V0.5.0 (November 2014). https://zenodo.org/record/12710#.W6C_32YcTIU. Accessed 6 Sept 2018
18. Reynolds Q, Erwee M, Moodley P (2018) Python-based machine learning tools for metallurgical data clustering. Paper presented at digitalization in mining conference, Sandton, South Africa, 6–7 June 2018
19. Jain AK (2010) Data clustering: 50 years beyond K-means. Pattern Recogn Lett 31(8):651–666
20. Pham DT, Dimov SS, Nguyen CD (2005) Selection of K in K-means clustering. Proc Institut Mech Eng Part C J Mech Eng Sci 219(1):103–119
21. Ding C, He X (2004) K-means clustering via principal component analysis. Paper presented at the twenty-first international conference on machine learning, Banff, Canada 4–8 July 2004
22. Al Shalabi L, Shaaban Z, Kasasbeh B (2006) Data mining: a preprocessing engine. J Comput Sci 2(9):735–739

23. Larose DT, Larose CD (2014) Discovering knowledge in data: an introduction to data mining. Wiley, New York
24. Shimura T, Kemp AI (2015) Tetrahedral plot diagram: A geometrical solution for quaternary systems. Am Miner 100(11–12):2545–2547
25. Jansson J, Taskinen P, Kaskiala M (2014) Freeze lining formation in continuous converting calcium ferrite slags. II. Canadian Metallurg Quarter 53(1):11–16
26. Crivits T, Hayes PC, Jak E (2018) An investigation of factors influencing freeze lining behaviour. Mineral Process Extract Metallurg 127(4):195–209
27. Voller VR (2009) Numerical methods for phase-change problems. In: Sparrow EM, Murthy JY (eds) Minkowycz, WJ. Handbook of numerical heat transfer. Wiley, Hoboken
28. Patankar SV (1980) Numerical heat transfer and fluid flow. Hemisphere Publishing Corporation, New York
29. Jones E, Oliphant T, Peterson P (2001) Scipy: open source scientific tools for Python. www.scipy.org. Accessed 6 Sept 2018
30. Bale CW et al (2016) FactSage thermochemical software and databases, 2010–2016. CALPHAD Comput Coupling Phase Diagr Thermochem 54:35–53
31. Routschka G, Wuthnow H (2008) Density. In: Refractory materials, 3rd ed. Vulkan Verlag, Essen
32. Routschka G, Wuthnow H (2008) Thermal conductivity. In: Refractory materials, 3rd ed. Vulkan Verlag, Essen
33. Perry RH, Green DW, Maloney JO (1997) Perry's chemical engineers' handbook. McGraw-Hill, New York
34. Xiao Y, Yang Y, Holappa LE (2006) Tracking chromium behaviour in submerged arc furnace for ferrochrome production. Presented at Sohn international symposium, San Antonio, USA, 12–16 Mar 2006
35. Bergmann C, Govender V, Corfield AA (2016) Using mineralogical characterisation and process modelling to simulate the gravity recovery of ferrochrome fines. Miner Eng 91:2–15
36. Holappa LE, Xiao Y (2004) Slags in ferroalloys production—review of present knowledge. J South Afr Inst Min Metall 104(7):429–437
37. Wilkerson KR et al (2013) Solid solution effects on the thermal properties in the $MgAl_2O_4$–$MgGa_2O_4$ system. J Am Ceram Soc 96(3):859–866
38. Kapralik I (1969) Thermal expansion of spinels $MgCr_2O_4$, $MgAl_2O_4$, and $MgFe_2O_4$. Chemické Zvesti 23(9):665–670
39. Duncanson PL, Toth JD (2004) The truths and myths of freeze lining technology for submerged arc furnaces. Paper presented at INFACON X, Cape Town, South Africa 1–4 Feb 2004